SCIEPublish

Communication

Mixed Matrix Membranes Produced from a Fluorinated MOF and Pebax for CO_2/H_2 Separation

Xiao-Yuan Chen and Denis Rodrigue *

Department of Chemical Engineering, Université Laval, Quebec, QC G1V 0A6, Canada;
xiao-yuan.chen.1@ulaval.ca (X.-Y.C.)

* Corresponding author. E-mail: denis.rodrigue@gch.ulaval.ca (D.R.)

Received: 6 July 2024; Accepted: 21 August 2024; Available online: 22 August 2024

ABSTRACT: Hydrogen (H_2) emerges as a promising clean energy source, but its efficient purification from various sources needs advanced separation technologies. This study explores the use of CO_2-selective membranes, especially mixed matrix membranes (MMM) incorporating KAUST-7 metal-organic framework (MOF), for hydrogen purification. The MMM was fabricated with various KAUST-7 content in a polymer matrix (Pebax 1657) and characterized via Fourier transform infrared spectroscopy (FTIR), scanning electron microscopy (SEM), thermogravimetric analysis (TGA), X-ray diffraction (XRD), and gas permeation tests. The XRD analysis confirms the incorporation of KAUST-7 into the MMM, while SEM reveals a homogeneous particle distribution at low content (below 10%) but agglomeration at higher ones (above 10%). FTIR confirms good interfacial interactions between the MOF and polymer matrix. TGA results show that the MMM thermal stability slightly decreases with increasing MOF content. Gas permeation results reveal improved CO_2 permeability (79%) and CO_2/H_2 selectivity (19%) for MMM compared to neat Pebax membranes, with an optimal performance observed at 10 wt.% KAUST-7. Beyond this threshold, the performance deteriorates, possibly due to polymer rigidity and MOF agglomeration. Overall, the study highlights the potential of KAUST-7/Pebax MMM for enhanced hydrogen purification.

Keywords: Mixed matrix membrane; Carbon dioxide; Hydrogen; Metal-organic framework; Pebax; KAUST-7; Permeability; Selectivity

1. Introduction

Hydrogen (H_2), known for its high calorific value for environmentally friendly combustion processes, stands out as a promising clean energy source [1–3]. Presently, H_2 is predominantly generated from two sources: syngas, which is a blend of H_2, CO, and CO_2 originating from feedstocks such as biomass, natural gas, heavy oil, and coal [1]; and biohydrogen, which is a compound comprising H_2, CO_2, and N_2, often having traces of elements such as H_2S and saturated with water [4]. In both cases, an additional purification step is required to meet industrial standards [1,5,6].

For CO_2/H_2 separation, and can be classified into two groups: H_2-selective membranes [7–11] and CO_2-selective membranes [12,13]. For pure gases, H_2 has a smaller kinetic diameter (2.89 Å) compared to CO_2 (3.30 Å); achieving preferential H_2 permeation is relatively straightforward. However, CO_2-selective membranes facilitate the passage of CO_2 and offer numerous advantages including separation costs, downstream uses, and membrane performances for industrial applications [14,15].

In the hydrogen purification from shifted synthesis gas and biohydrogen process, CO_2-selective membranes function as reverse-selective membranes, allowing larger CO_2 molecules to permeate faster than smaller H_2 molecules [5,16]. To achieve a preference for CO_2 permeation, these membranes must exhibit a strong affinity for CO_2. This requirement is controlled by the high condensability and acidic nature of the CO_2 molecule.

Currently, CO_2-selective membranes come in several types, including microporous membranes (SAPO-34 membrane and polymers of intrinsic microporosity or PIM), CO_2-philic polymeric membranes, and mixed matrix membranes (MMM) [13]. Polymeric membranes for CO_2 selectivity aim to increase the CO_2/H_2 solubility-selectivity by introducing polar functional groups and decreasing the H_2/CO_2 diffusivity-selectivity by modifying the chain packing.

https://doi.org/10.35534/ces.2024.10015

Poly(ethylene oxide) (PEO), also known as poly(ethylene glycol) (PEG), with low molecular weight (less than 1500 g/mol), is commonly used in CO_2-philic polymeric membranes, often in copolymer blending systems. Commercially available copolymers, such as Pebax (poly(ether-*b*-amide, HO-(CO-PA-CO-O-PE-O)n-H), are extensively used as matrices [17–20].

Mixed matrix membranes are made from a polymer matrix and nanofillers and were shown to have good properties as CO_2-selective membranes [21–23]. The polymer matrix generates excellent mechanical/rheological properties for membrane fabrication and operation/handling [23,24]; while the nanofillers (zeolite molecular sieves [25–27]), metal-organic frameworks (MOF) [28,29], and covalent organic frameworks (COF) [30–33], create porous channels for gas transport.

Li et al. (2011) developed MMM at the molecular level using Pebax MH 1657 with two types of POSS (polyhedral oligomeric silsesquioxane) cages: amic acid-functionalized POSS and hydroxyl group-functionalized POSS [34]. For low filler content (2–3 wt.%), they observed an improvement in both CO_2 permeability and CO_2/H_2 selectivity due to higher free volume. However, the performance declined at higher contents as the polymer chains became more rigid. The best CO_2/H_2 selectivity obtained was 8.4–8.8 coupled with a CO_2 permeability of 108–127 Barrer at 8 bar and 308 K.

Zhao et al. (2013) incorporated amino group-functionalized multi-walled carbon nanotubes (MWCNT) into Pebax MH 1657 [35]. The gas permeability (360 Barrer) was found to increase with higher filler content (33 wt.% of MWCNT-NH_2) without significant modification of the CO_2/H_2 selectivity [9].

KAUST-7, also known as NbOFFIVE-1-Ni, was first synthesized by Eddaoudi and co-workers in 2016 using a co-solvent method [36]. This material consists of Ni(II)-pyrazine square grid layers with (NbOF5)2–pillars showing exceptional sorption selectivity for CO_2 over N_2, CH_4 and H_2. Featuring an ultra-micro aperture size of around 3.5 Å, KAUST-7 holds promise for CO_2 separation from natural gas or flue gas related to kinetic separation principles. However, the large crystals reported (~30 μm) were unsuitable to prepare high-quality MMM [37]. To overcome this limitation, nano-sized (<100 nm) KAUST-7 crystals having a uniform particle size distribution were effectively used as a CO_2-philic MOF to prepare MMM for different gases, such as CO_2/CH_4 separation [38], as well as the removal of CO_2 and H_2S from natural gas [39].

Chen et al. [38] produced MMM using KAUST-7 and 6FDA-durene (6FDA: 4,4′-(hexafluoroisopropylidene) diphthalic anhydride) for CO_2/CH_4 separation. In this case, significant improvements for CO_2/CH_4 selectivity and CO_2 permeability were reported, and the basic principles are presented in Figure 1. Compared to neat 6FDA-durene membranes, a MMM containing 33 wt.% KAUST-7 nanocrystals showed a 36% increase in CO_2 permeability and a 50% increase in CO_2/CH_4 selectivity related to the improved sorption selectivity generated.

Liu et al. [39] prepared MMM using several fluorinated MOF, NbOFFIVE-1-Ni (KAUST-7), AlFFIVE-1-Ni with 6FDA-DAM (DAM: 2,4,6-trimethyl-1,3-diaminobenzene) for $H_2S/CO_2/CH_4$ separation. The test condition was a very aggressive model natural gas feed (20% H_2S, 20% CO_2 and 60% CH_4) and at 6.9 bar, 35 °C. The removal performance of the MMM was reported based on the total acid gas permeability [$P_{(CO2)} + P_{(H2S)}$] and selectivity [$P_{(CO2)} + P_{(H2S)}$]/$P_{(CH4)}$. The separation of 6FDA-DAM membrane (672 Barrer and 39.7 selectivity) was highly improved by adding 20 wt.% NbOFFIVE-1-Ni (948 Barrer and 48.9 selectivity) or 20 wt.% AlFFIVE-1-Ni (1047 Barrer and 42.4 selectivity). These fluorinated MOF-based membranes were shown to have excellent CO_2 capture properties.

As a rubbery polymer, the block copolymer Pebax MH 1657, comprises two parts: a 60% polyethylene oxide (PEO) section and a 40% polyamide (PA) section. The PEO block provides a strong affinity with CO_2 due to quadrupole–dipole interaction, while the PA block offers good mechanical properties. Good interfacial interaction with the OH groups in PA can attract the hydrogen (H) of the pyrazine part in KAUST-7, enhancing the compatibility inside the MMM.

Based on the information from the literature, using KAUST-7 MOF as a CO_2-philic represents an interesting possibility to increase the separation performances of mixed matrix membranes (MMM) designed for hydrogen purification. The strong affinity of KAUST-7 MOF towards carbon dioxide molecules facilitates their selective adsorption and separation from hydrogen gas streams (Figure 1). When incorporated into MMM, KAUST-7 MOF can significantly enhance the gas separation properties, especially regarding CO_2 capture efficiency and permeability. Its high surface area and tunable pore structure provide efficient gas diffusion and adsorptionand opportunities leading to improve membrane performance. Additionally, the compatibility between KAUST-7 MOF and CO_2-philic polymers, such as Pebax (poly(ether-block-amide)), ensures excellent interfacial adhesion and compatibility within the polymer matrix. This synergistic combination of CO_2-philic MOF and polymer constituents results in MMM with enhanced selectivity, permeability, and mechanical strength, making them well-suited for membrane-based hydrogen purification applications. So, the objective is to determine the effect of KAUST-7 concentration on the properties of Pebax for CO_2/H_2 separation.

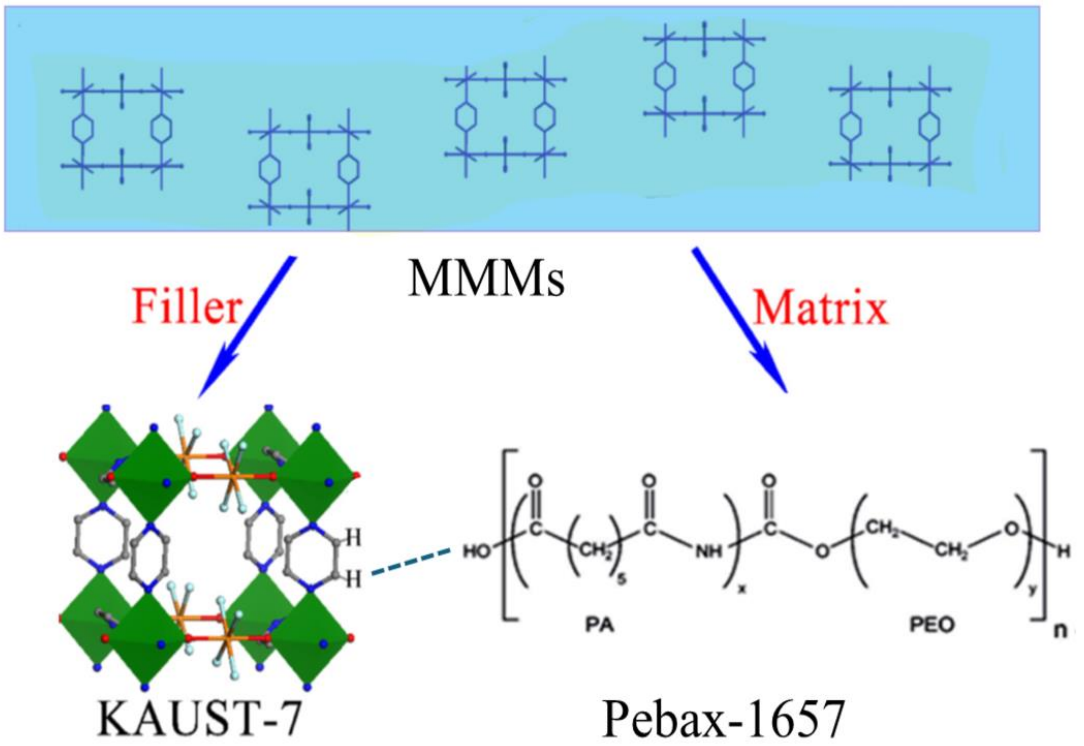

Figure 1. Structures of KAUST-7/Pebax MH 1657 mixed matrix membrane (MMM). Oxygen (O): Red; Nitrogen (N): Blue; Carbon (C): Dark gray; fluorine (F): light blue, Nickel (Ni): Gold-colored; Niobium (Nb): green polyhedral shapes (octahedral structures) in the KAUST-7 MOF.

2. Experimental

2.1. Materials

Pebax® MH 1657 (Arkema Inc., King of Prussia, PA, USA) was used as received in pellet form. Ethanol (95% purity), supplied by GreenField Specialty Alcohols Inc. (Mississauga, ON, Canada), was used to prepare the samples via solvent casting. KAUST-7 nanocrystals were provided by the Eddaoudi group at King Abdullah University of Science and Technology (Thuwal, Saudi Arabia).

2.2. Fabrication of Mixed Matrix Membrane

To prepare neat membranes, a 5 wt.% solution of Pebax in a mixture of 30% distilled water and 70% ethanol was continuously mixed for 4 h at 90 °C under reflux. Subsequently, the solution was cast into a Teflon dish, and solvent evaporation took place for 48 h at room temperature. A thin sheet of paper was placed on top to control the evaporation rate. Then, the membranes were placed overnight in a vacuum oven (60 °C) to eliminate the remaining solvent. The resulting membrane was transparent and uniform, with a thickness of 50–70 microns. For the mixed matrix membranes (MMM), various MOF contents (5, 10, 15, and 20 wt.%) were dispersed into the solvent via continuous mixing for 2 h at 90 °C under reflux. Next, the solution was placed into a sonication bath and sonicated (30 min). Half of the polymer was then added and mixed under the same conditions. After 12 h, the solution underwent another 30 min of sonication. Subsequently, the other half of the polymer was added and the solution was continuously mixed under the same conditions for 24 h. A final 30 min of sonication was performed and the solution was rapidly cast before drying as described.

2.3. Characterization

The KAUST-7 crystals and MMM structure were determined via X-ray diffraction (Rigaku Smartlab TM 9 kW powder diffractometer at 40 kV, 40 mA) using CuKα as a source of radiation.

Fourier transform infrared (FTIR) spectra were obtained by scanning (400 to 4000 cm^{-1}). A Nicolet iS10 FTIR spectrometer was combined with an attenuated transmission (ATR) accessory. A total of 128 scans were used to average the spectra with a resolution of 4 cm^{-1}.

The morphologies/structures of the KAUST-7 crystals and membranes were characterized (different magnifications) via scanning electron microscopy (SEM) using an Inspect F50 (FEI, Hillsboro, OR, USA) at 15–20 kV. The membrane cross-section was exposed via cryogenic fracture (liquid nitrogen) before sputter-coating with palladium.

Thermogravimetric analysis (TGA) was used to determine the stability from a Q5000IR (TA Instruments, New Castle, DE, USA). The tests were done in nitrogen between 50 and 800 °C with a heating rate of 10 °C/min.

2.4. Gas Permeation Test

The gas transport properties were determined using a variable pressure (constant volume) setup. The initial test focused on single-gas permeation and was conducted using a home-made setup, as detailed in a prior publication [40]. Circular membranes (42 mm in diameter) were positioned within a blind flange and secured using silicone rings. The permeation setup was placed in a temperature-controlled oven. Each side of the membrane was subjected to evacuation for 1–2 h at either 35 or 55 °C, followed by a leak test to ensure integrity. Before starting, the permeation gas was placed on one side at 2 bar while the other remained under continuous evacuation (vacuum). Subsequently, the pressure (p) on the permeate side was measured until steady-state. The slope (dp/dt) (cmHg s^{-1}) was then used to calculate the permeability in Barrer (10^{-10} cm^3 (STP)cm cm^{-2} s^{-1} $cmHg^{-1}$) as:

$$P = \frac{22414}{A} \times \frac{V}{RT} \times \frac{l}{\Delta p} \times \frac{dp}{dt} \quad (1)$$

where A is the membrane surface (14.5 cm^2), V is the volume on the permeate side (cm^3), R is the gas constant (6236.56 cm^3 cmHg mol^{-1} K^{-1}), T is the temperature (K), l is the membrane thickness (cm), and $\triangle p = (p_2 - p_1)$ where p_1 and p_2 are the permeate pressure and feed pressure (psi) respectively. The ideal selectivity (α_{AB}) is determined from single gas permeability (P) measurements. It represents the ratio between the most permeable gas (A) and the least permeable one (B):

$$\alpha_{AB} = \frac{P_A}{P_B} \quad (2)$$

3. Results and Discussion

3.1. XRD Analysis

The XRD (X-ray diffraction) analysis depicted in Figure 2 reveals crucial insights into the structural characteristics of the mixed matrix membranes (MMM) containing KAUST-7 MOF. In particular, the diffraction peaks observed in the XRD patterns of the MMM align well with the diffraction peaks expected for the crystalline structure of KAUST-7 MOF, as evidenced by the prominent peak at 2Θ (angle of diffraction) around 12.5° [36]. Furthermore, an intriguing observation from the XRD analysis is the gradual broadening and weakening of the characteristic peaks as the KAUST-7 MOF content increases. This phenomenon is noteworthy when compared to the peak intensity and width of the neat KAUST-7 crystals.

Peak broadening in XRD patterns suggests a reduction in the crystallite size or an increase in structural disorder within the MMM due to KAUST-7 MOF incorporation. This could be attributed to the interaction between the polymeric matrix and MOF, generating a more disordered arrangement of MOF crystallites inside the composite material.

Moreover, the weakening of the characteristic peak (12.6°) indicates a decrease in the crystallinity of the MMM relative to the neat KAUST-7 crystals. This can be related to the disruption of the MOF crystallinity caused by its dispersion inside the polymer and potential interfacial interactions between the polymer and MOF [41].

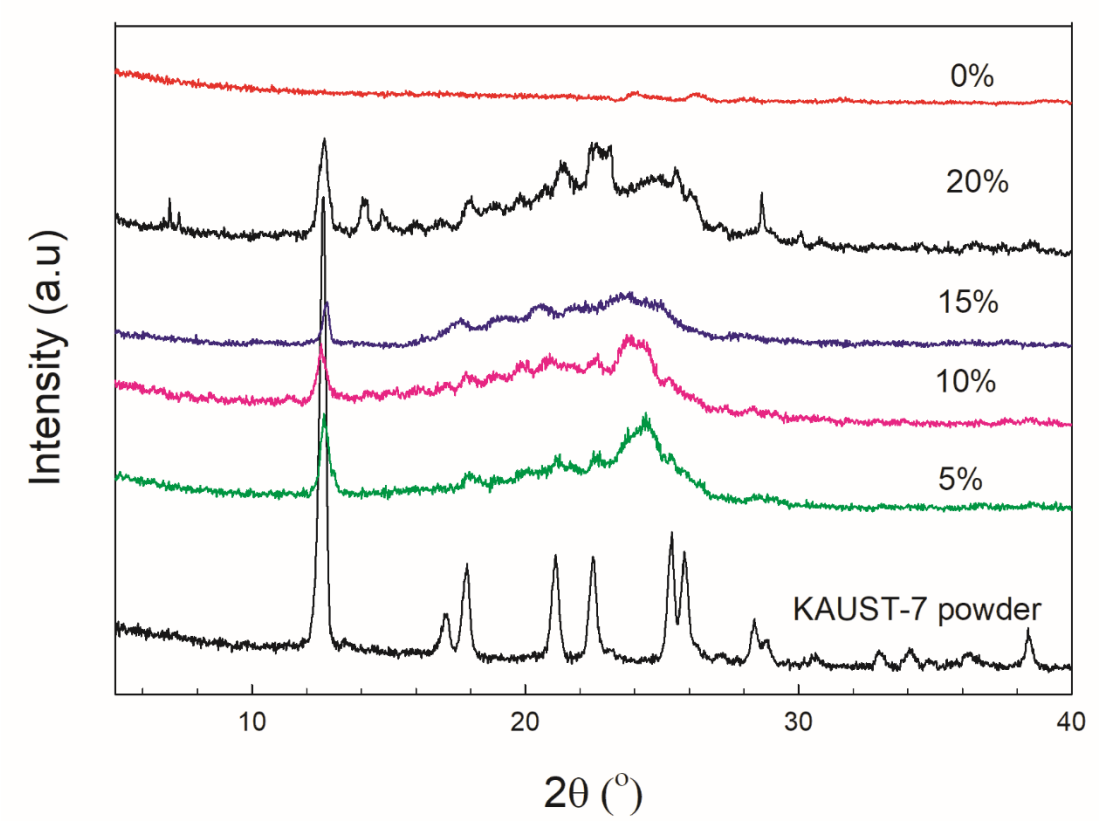

Figure 2. X-ray diffraction (XRD) patterns of KAUST-7 powder, Pebax 1657 and the MMM (5, 10, 15 and 20 wt.%).

3.2. SEM Analysis

Metal–organic frameworks (MOF) are modular and tunable highly crystalline porous materials [38]. Figure 3 presents typical SEM micrographs of the KAUST-7 powder. The images confirm that the particle sizes are less than 100 nm, while their agglomerations can be up to several microns in size [38,39].

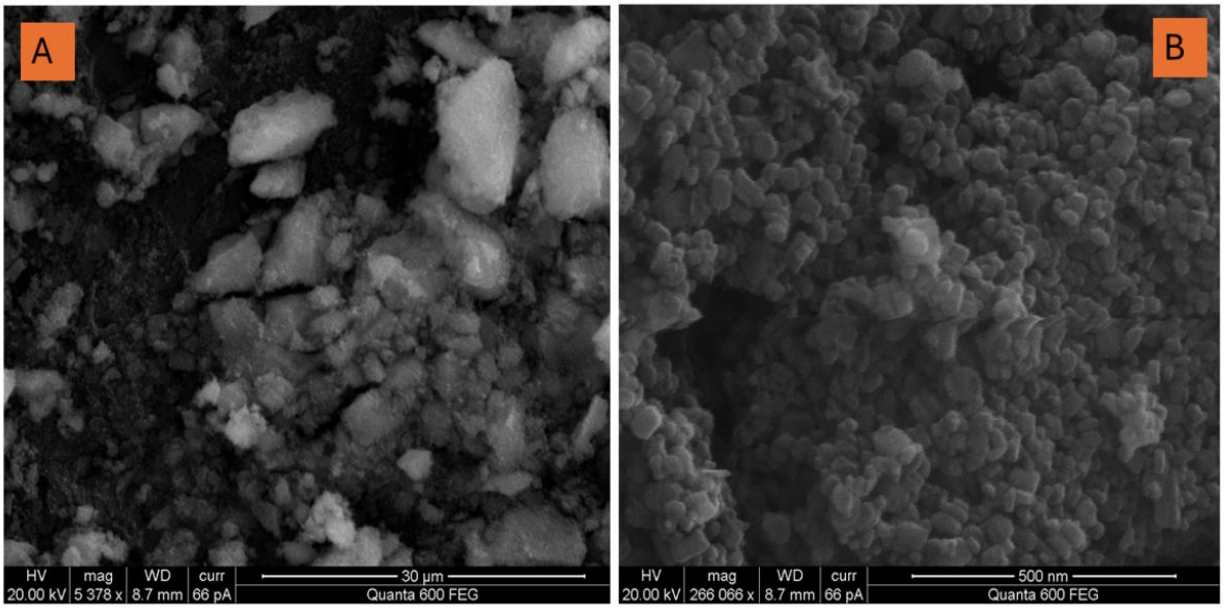

Figure 3. SEM images of the MOF (KAUST-7) at different magnification: (**A**) 5378× and (**B**) 266,066×.

Figure 4 presents typical images of the MMM for various KAUST-7 concentrations. The membrane thickness is 90–120 microns.

For the neat Pebax membrane (Figure 4A), the image shows that the matrix is without voids or defects and exhibits a smooth surface texture. This membrane serves as the base material for the MMM. The structure gets more textured

when adding low KAUST-7 nanocrystals (Figure 4B,C). At low KAUST-7 content (5 and 10 wt.%), the SEM images show a homogeneous MOF distribution throughout the polymer. This uniform dispersion suggests efficient mixing and interaction between the MOF nanoparticles and Pebax. Upon closer examination at higher magnification, the MOF nanocrystals are well-embedded within the Pebax matrix without visible defects or voids observed. This "sieve-in-a-cage" structure indicates that the MOFs are encapsulated or surrounded by the polymer, enhancing their dispersion and minimizing the possibility of particle detachment or aggregation. Additionally, a polymer network of a circular pattern (morphology) is another confirmation of good interfacial interaction [40]. However, at higher KAUST-7 content (20 wt.% in Figure 4D), the image reveals notable differences compared to lower concentrations. In this case, clusters or agglomerates of KAUST-7 nanocrystals become apparent within the matrix. This aggregation may lead to non-uniform properties within the MMM, affecting its overall performance. The presence of agglomerated nanofillers alters the MMM morphology, creating irregularities in the structure. This non-uniform morphology can lead to variations in mechanical strength and gas transport properties, affecting the overall MMM performance. In regions where nanofillers agglomerate, voids or gaps are seen in the matrix, compromising the MMM's structural integrity and barrier properties (preferential channel) potentially leading to decreased performance or failure under lower stress conditions.

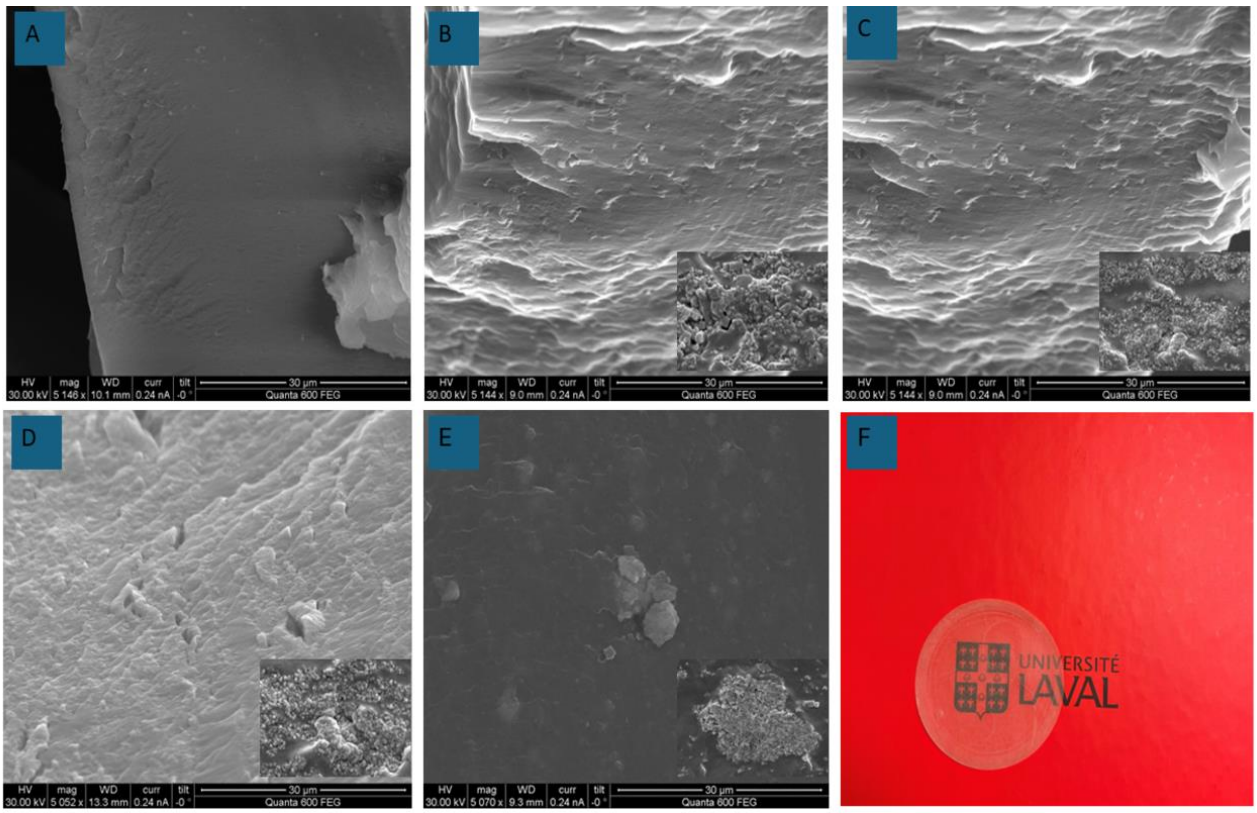

Figure 4. SEM images of the MMM with: (**A**) 0, (**B**) 5, (**C**) 10, (**D**) 15 and (**E**) 20 wt.% KAUST-7, (**F**) 15 wt.% KAUST-Pebax membrane.

3.3. FTIR Analysis

To confirm the MOF inclusion in the matrix, FTIR was done and the spectra are reported in Figure 5. The typical Pebax bands are located at 845 cm^{-1} due to –OH stretching, 1099 cm^{-1} and 1734 cm^{-1} related to –C=O (saturated ester groups) and –O–C– (EO segments) [42]. The peaks at 1099 cm^{-1} and 1734 cm^{-1} (PEO segments of Pebax and saturated ester groups) are shifted to lower frequencies with lower intensity and higher MOF concentration. For the MMM, the appearance of Nb–O stretching (480 cm^{-1}), Ni–N stretching (450 cm^{-1}), and C=N from pyrazine (1473 cm^{-1}) indicate the presence of KAUST-7. Bands shifting indicates good affinity and strong chemical interactions [43]. This confirms that hydrogen bonding occurs between the H of the pyrazine in KAUST-7 and the EO segments of Pebax. This is why good interaction between both phases was obtained without interfacial defects (Figure 4).

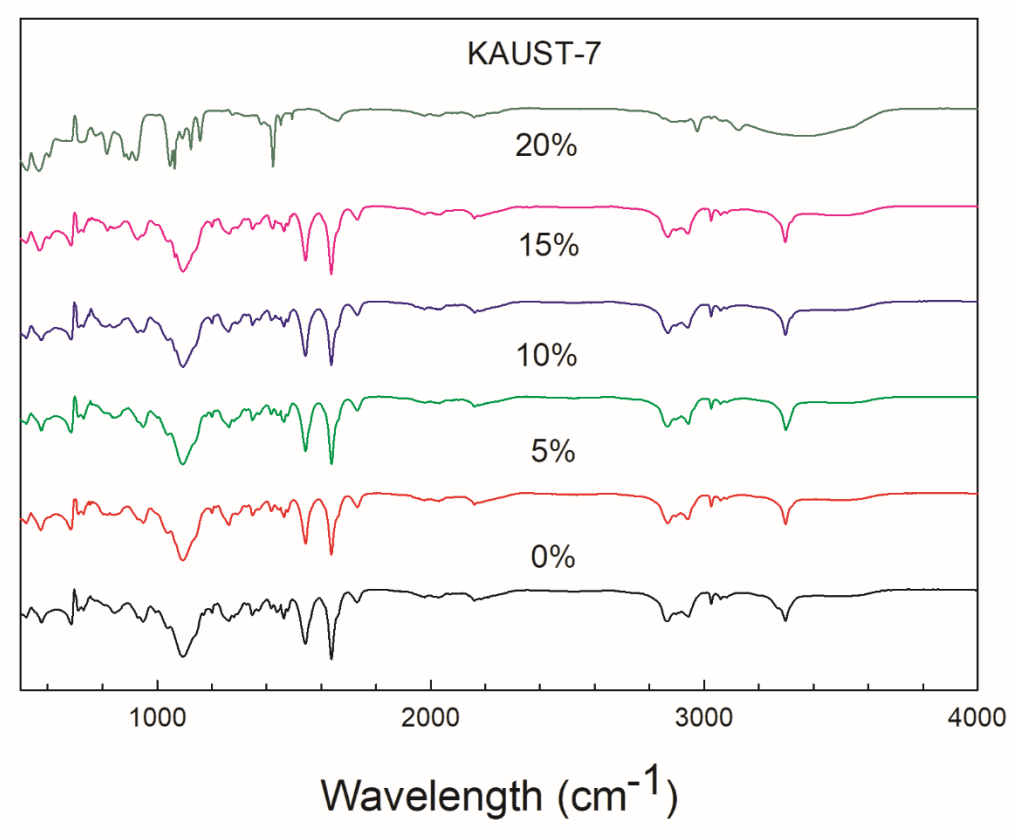

Figure 5. FTIR spectra of KAUST-7 powder, Pebax 1657, and typical MMM (5, 10, 15 and 20 wt.%).

3.4. Thermal Analysis

TGA-DTG results were used to determine the thermal stability of the materials (Figure 6). Table 1 presents the temperatures derived from the TGA curves from the first peak in the DTG curves. Typically, temperatures at which 5% ($T_{d5\%}$) and 10% ($T_{d10\%}$) weight loss occur are reported (Table 1). These curves also provide insights into the degradation rates. The results of Figure 6A show that KAUST-7 has a much lower thermal stability than Pebax as its $T_{5\%}$ is 265 °C lower (63 vs. 328 °C). This is why the MMM is less stable with increasing MOF content.

Table 1. Characteristic temperatures (°C) obtianed from TGA-DTG curves.

Sample	KAUST-7 Content (wt.%)	$T_{d5\%}$ (°C)	$T_{d10\%}$ (°C)	Residues (%)
KAUST-7	100	63	92	45.4
Pebax	0	328	360	2.6
MMM	5	264	303	6.7
	10	255	303	7.4
	15	234	302	8.4
	20	181	301	9.5

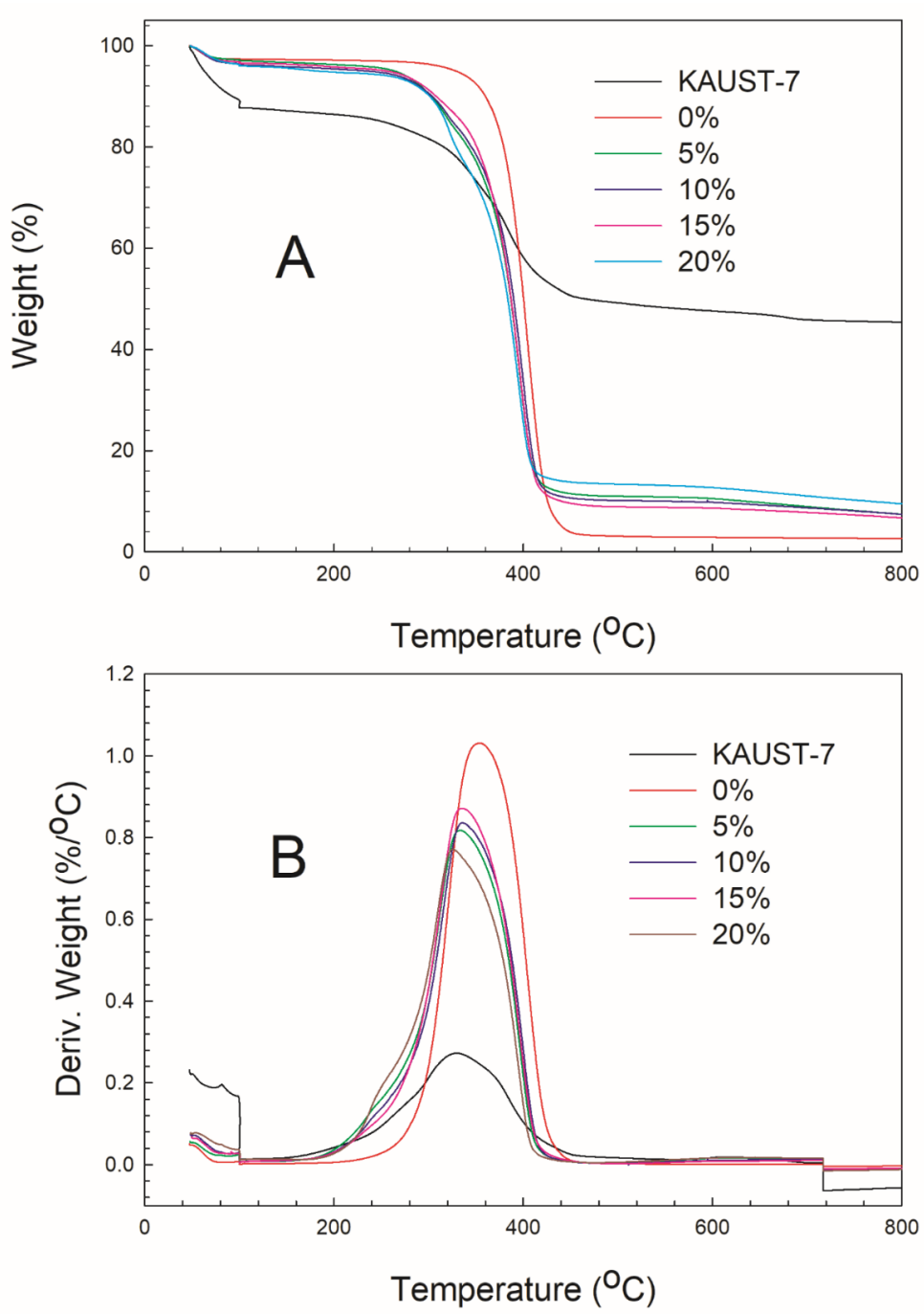

Figure 6. (**A**) TGA and (**B**) DTG curves of KAUST-7 powder, Pebax 1657 and the MMM (5, 10, 15 and 20 wt.%).

Figure 6A also shows that KAUST-7 exhibits a distinct weight loss pattern, elucidated by TGA and DTG plots. Initially, the sample undergoes water loss between 30 °C and 150 °C, with a notable decline at 100 °C (Figure 6B-DTG), followed by a plateau extending from 150 °C to 250 °C. The first 8% weight loss (20 °C to 250 °C) corresponds to the loss of two water (7.8 wt.%). Notably, material decomposition initiates above 250 °C, with a prominent peak at 328 °C followed by a smaller one at 720 °C [38]. Despite its decomposition, the metal element content persists, resulting in residues comprising 45% wt.

The neat Pebax presents excellent thermal properties since its melting point is around 159 °C. It is also very stable for high-temperature use, as evidenced by its high $T_{d5\%}$ and $T_{d10\%,}$ reaching 328 °C and 360 °C, respectively.

For the MMM, negligible weight loss is observed up to 250 °C, suggesting an effective removal of most casting solvents (water and ethanol) through the vacuum drying protocol. Consequently, the onset degradation temperatures marginally decrease with increasing MOF content ($T_{d5\%}$,$T_{d10\%}$ in Table 2). This trend is expected as higher MOF content leads to increased material degradation, consistent with observations for other MOFs ($Cu_3(BTC)_2$, UiO-66-NH_2 and MIL-53-NH_2) [43]. Nevertheless, all the MMM have good thermal resistance as their $T_{5\%}$ are all above 181 °C, which is much higher than the normal operating conditions for membrane gas separation.

3.5. Gas Permeation Analysis

The permeability for H_2 and CO_2 was determined at 2 bar for two temperatures (35 and 55 °C). The effect of temperature and MOF content are presented in Table 2 and Figure 7. The performances of the neat matrix and MMM were obtained by permeation tests. Based on Table 2 and Figure 7, all the MMM have higher CO_2, H_2 and CO_2/H_2 ideal selectivity compared to the neat matrix. This is expected because KAUST-7 features an ultra-micro aperture size (3.5 Å) and is CO_2-philic. Although H_2 and CO_2 molecules can pass through the MOF, CO_2 permeation is favorized.

Table 2. Permeability (Barrer) and selectivity (-) of the MMM.

MMM (KAUST wt.%)	P_{CO2}	SD *	P_{H2}	SD	P_{CO2}/P_{H2}	SD	Test Conditions
0	91	1	10.2	0.1	8.9	0.1	35 °C and 2 bar
5	146	1	14.7	0.3	9.8	0.1	
10	163	8	16.2	0.5	10.1	0.2	
15	115	2	10.9	2.4	10.6	0.1	
0	136	3	27.5	1.5	4.9	0.2	55 °C and 2 bar
5	209	1	32.3	0.2	6.4	0.1	
10	229	2	36.6	0.5	6.4	0.1	
15	176	1	27.5	1.5	6.3	1.1	

* SD = standard deviation.

All the MMM permeabilities are above the neat matrix and increase to a critical MOF content (10 wt.%). This is in agreement with several previous works. Meshkat et al. [43] observed that 10 wt.% was the optimum content for NH_2-MIL-53 in Pebax, leading to a 174% increase in CO_2 permeability over the neat matrix, while Tien-Binh et al. [44] observed that 10–15 wt.% was the optimum MIL-53 concentration in 6FDA-DAM for CO_2/CH_4 separation with 46–47 Barrer of CO_2 permeability and 58–78 of selectivity.

These results show that the CO_2 permeability of 10% KAUST-7/Pebax 1657 MMM is 79% and 68% higher than the neat matrix at 35 and 55 °C, respectively, while the H_2 permeabilities are also above the neat matrix values because of MMM porosity. However, in this case, the increases are lower (Table 2). Therefore, the ideal selectivity for CO_2/H_2 was improved by 14% and 29% at 35 and 55 °C, respectively.

Nevertheless, the permeability drops at 15% KAUST-7 because of a rigid polymer layer around the MOF and the tortuosity associated with the rigid particles generating lower gas molecules mobility to a high volume of the porosity. When the MOF content reaches 20%, MOF agglomeration generates membranes becoming too rigid and easy to break so that no data can be obtained.

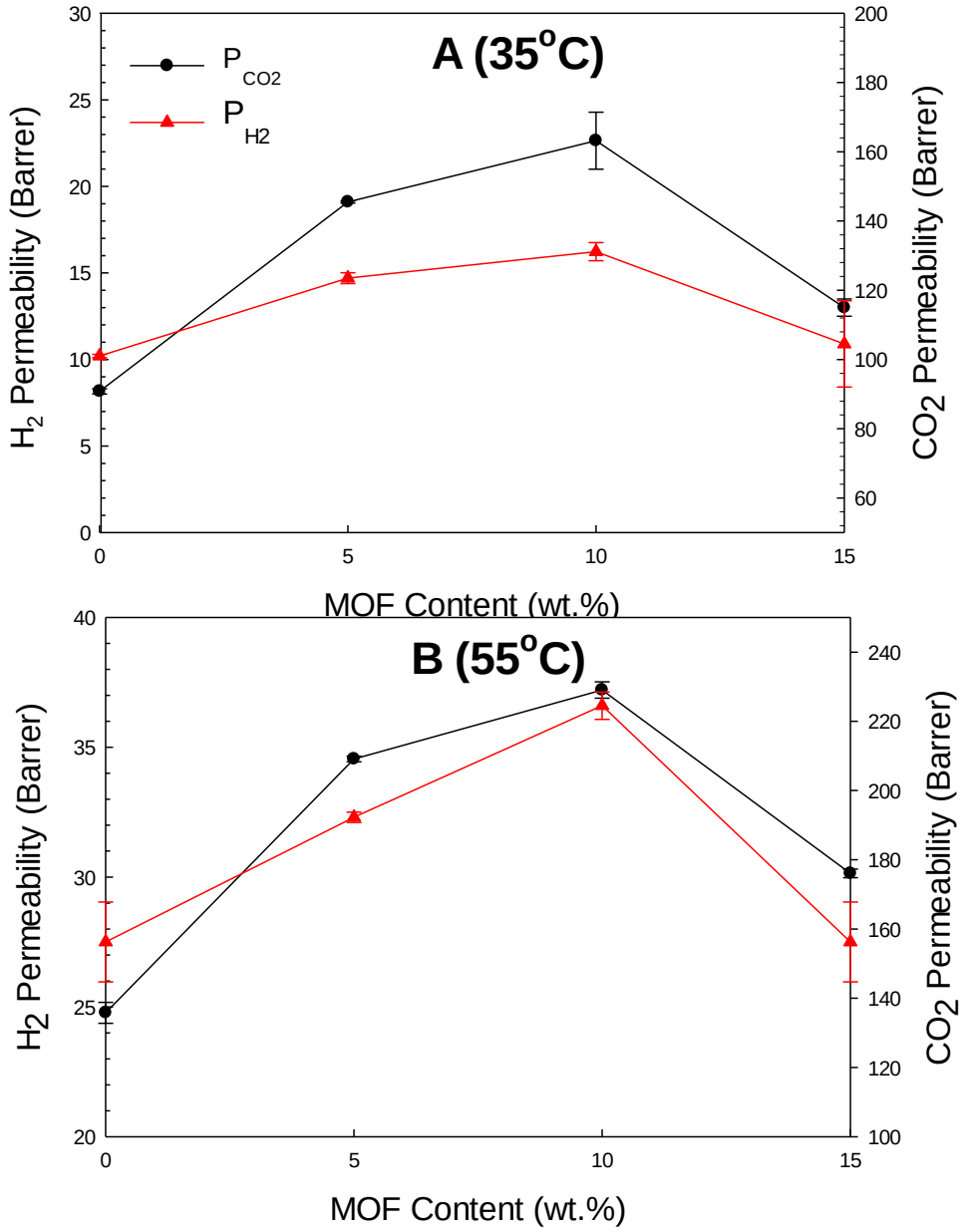

Figure 7. Gas permeation properties of KAUST-7/Pebax 1657 MMM at P = 2 bar under different temperature: (**A**) 35 °C and (**B**) 55 °C.

3.6. Comparison of CO_2-Selective MMM

Usually, gas separation performances for polymer membranes are compared based on Robeson's upper bounds [45], but the results are only presented for H_2/CO_2 and not for CO_2/H_2 separation. This is why Figure 8 reports the properties of CO_2-selective membranes compared with the upper bound proposed by Freeman [46]. It can be seen that few CO_2-selective mixed matrix membranes have been studied to compare the CO_2/H_2 selectivity.

Nevertheless, some CO_2-selective MMM have been investigated, including PI-Zeolite-5 MMM comprising polyimide (PI-6FDA-TeMPD) with 15 wt.% zeolite (ZSM-5) in liquid sulfolane (SF) [47], Pebax-SAPO-34 MMM with 23% nanofiller [48] and 8 wt.% SiO_2 [49], Pebax MH 1657 with amino group-functionalized MWCNT [33], poly(ethylene oxide) (PEO)-silica of 10 wt.% [50], polyetheramine (PEA)-polyhedral oligomeric silsesquioxane (POSS) MMM [51], Pebax® 1657 with ZIF-8 particles [52], and azide crosslinked poly(4-methyl-1-pentyne) (PMP) MMM with nano-CuBTC MOF [53]. While some membranes showed enhanced gas permeability with increased filler content, but the CO_2/H_2 selectivity remains unchanged. The conditions also vary across the studies, with temperature and pressure playing significant roles in membrane performance. Finally, these findings underscore the need for tailored MMM design to optimize the CO_2 separation efficiency for diverse industrial applications.

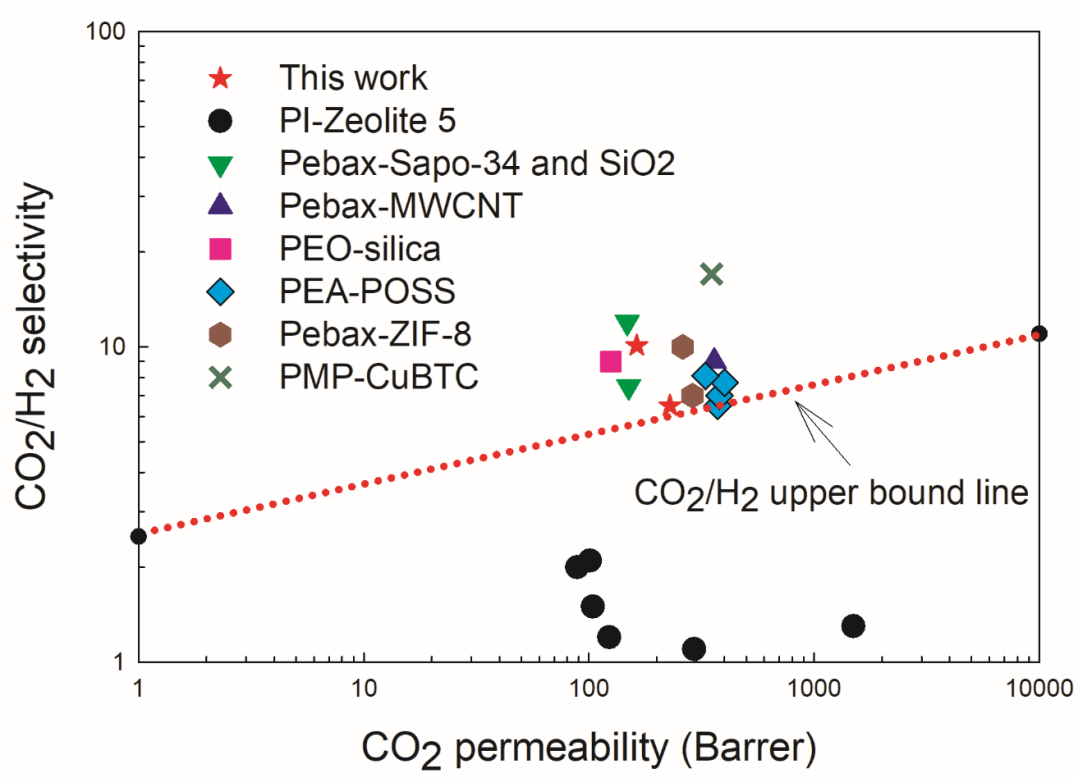

Figure 8. Comparison between the membranes prepared (163 Barrer/10.1 of selectivity; 229 Barrer/6.4 of selectivity) with the upper bound [46] and MMM from the literature [35,47–53] for CO_2/H_2 gas separation.

4. Conclusions

Incorporating KAUST-7 MOF in Pebax MH 1657 to form mixed matrix membranes (MMM) presents a promising approach for hydrogen purification. This study confirmed that MMM based on KAUST-7 exhibited enhanced CO_2/H_2 selectivity and CO_2 permeability compared with the neat matrix (79% and 14% at 35 °C; 68% and 29% at 55 °C), especially for the optimal MOF content (10 wt.%). However, the performance decreased beyond this threshold due to potential factors such as polymer rigidity and MOF agglomeration. Nevertheless, the strong interfacial interactions confirmed by FTIR and the thermal stability observed in TGA suggest the viability of KAUST-7/Pebax MMM for practical gas separation applications. Further optimization and scale-up efforts could be made to develop improved polymer membranes in the field of efficient hydrogen purification under industrial settings. Finally, more work is needed to measure the membranes' mechanical properties, especially their stability (long-term properties).

Acknowledgments

The authors want to thank King Abdullah University of Science and Technology (KAUST, Saudi Arabia) for a six-month internship (X.-Y. Chen) and Dr. Osama Shekhah for providing the MOF (KAUST-7) used in this work.

Author Contributions

Conceptualization, D.R. and X.-Y.C.; methodology, X.-Y.C.; Software, X.-Y.C.; formal analysis, X.-Y.C.; investigation, X.-Y.C.; resources, D.R.; data curation, X.-Y.C.; writing—original draft preparation, X.-Y.C.; writing—review and editing, D.R.; visualization, X.-Y.C.; supervision, D.R.; project administration, D.R.; funding acquisition, D.R. All authors have read and agreed to the published version of the manuscript.

Ethics Statement

Not applicable.

Informed Consent Statement

Not applicable.

Funding

This research received no external funding.

Declaration of Competing Interest

The authors declare no conflict of interest.

References

1. Turner JA. Sustainable hydrogen production. *Science* **2004**, *305*, 972–974.
2. Lau CH, Li P, Li FY, Chung TS, Paul DR. Reverse-selective polymeric membranes for gas separations. *Prog. Polym. Sci.* **2013**, *38*, 740–766.
3. Hosseini SE, Wahid MA. Hydrogen production from renewable and sustainable energy resources: Promising green energy carrier for clean development. *Renew. Sustain. Energy Rev.* **2016**, *57*, 850–866.
4. Bakonyi P, Nemestothy N, Belafi-Bako K. Biohydrogen purification by membranes: An overview on the operational conditions affecting the performance of non-porous, polymeric and ionic liquid-based gas separation membranes. *Int. J. Hydrogen Energy* **2013**, *38*, 9673–9687.
5. Lin H, He Z, Sun Z, Vu J, Ng A, Mohammed M, et al. CO_2-selective membranes for hydrogen production and CO_2 capture—Part I: Membrane development. *J. Membr. Sci.* **2014**, *457*, 149–161.
6. Ockwig NW, Nenoff TM. Membranes for hydrogen separation. *Chem. Rev.* **2007**, *107*, 4078–4110.
7. Wu J, Liang CZ, Naderi A, Chung TS. Tunable Supramolecular Cavities Molecularly Homogenized in Polymer Membranes for Ultraefficient Precombustion CO_2 Capture. *Adv. Mater.* **2022**, *34*, 2105156.
8. Wu J, Chung TS. Supramolecular Polymer Network Membranes with Molecular-Sieving Nanocavities for Efficient Pre-Combustion CO_2 Capture. *Small Methods* **2022**, *6*, 2101288.
9. Feng F, Wu J, Liang CZ, Weber M, Zhang S, Chung TS. Synergistic dual-polymer blend membranes with molecularly mixed macrocyclic cavitands for efficient pre-combustion CO_2 capture. *Chem. Eng. J.* **2023**, *470*, 144073.
10. Lv JY, Zhou XR, Yang JH, Wang L, Lu JM, He GH, et al. In-situ synthesis of KAUST-7 membranes from fluorinated molecular building block for H_2/CO_2 separation. *J. Membr. Sci.* **2022**, *658*, 120585.
11. Japip S, Liao KS, Chung TS. Molecularly tuned free volume of vapor cross-linked 6FDA-durene/ZIF-71 MMM for H_2/CO_2 separation at 150 °C. *Adv. Mater.* **2017**, *29*, 1603833.
12. Kang ZX, Peng YW, Qian YH, Yuan DQ, Addicoat MA, Heine T, et al. Mixed matrix membranes (MMM) comprising exfoliated 2D covalent organic frameworks (COFs) for efficient CO_2 separation. *Chem. Mater.* **2016**, *28*, 1277–1285.
13. Li PY, Wang Z, Qiao ZH, Liu YN, Cao XC, Li W, et al. Recent developments in membranes for efficient hydrogen purification. *J. Membr. Sci.* **2015**, *495*, 130–168.
14. Lin H, He Z, Sun Z, Kniep J, Ng A, Baker RW, et al. CO_2-selective membranes for hydrogen production and CO_2 capture—Part II: Techno-economic analysis. *J. Membr. Sci.* **2015**, *493*, 794–806.
15. Vakharia V, Ramasubramanian K, Ho WSW. An experimental and modeling study of CO_2-selective membranes for IGCC syngas purification. *J. Membr. Sci.* **2015**, *488*, 56–66.
16. Shao L, Low BT, Chung TS, Greenberg AR. Polymeric membranes for the hydrogen economy: Contemporary approaches and prospects for the future. *J. Membr. Sci.* **2009**, *327*, 18–31.
17. Yave W, Car A, Peinemann KV, Shaikh MQ, Rätzke K, Faupel F. Gas permeability and free volume in poly(amide-b-ethyleneoxide)/polyethylene glycol blend membranes. *J. Membr. Sci.* **2009**, *339*, 177–183.
18. Yave W, Car A, Peinemann KV. Nano structured membrane material designed for carbon dioxide separation. *J. Membr. Sci.* **2010**, *350*, 124–129.
19. Ghadimi A, Amirilargani M, Mohammadi T, Kasiri N, Sadatnia B. Preparation of alloyed poly(etherblockamide)/poly(ethylene glycol diacrylate) membranes for separation of CO_2/H_2 (syngas application). *J. Membr. Sci.* **2014**, *458*, 14–26.
20. Rabiee H, Soltanieh M, Mousavi SA, Ghadimi A. Improvement in CO_2/H_2 separation by fabrication of poly(ether-b-amide6)/glycerol triacetate gel membranes. *J. Membr. Sci.* **2014**, *469*, 43–58.
21. Patel NP, Miller AC, Spontak RJ. Highly CO_2-permeable and selective polymer nanocomposite membranes. *Adv. Mater.* **2003**, *15*, 729–733.
22. Qiao ZH, Sheng ML, Wang JX, Zhao S, Wang Z. Metal-induced polymer framework membrane with high performance for CO2 separation. *AIChE J.* **2019**, *65*, 239–249.
23. Dechnik J, Gascon J, Doonan CJ, Janiak C, Sumby CJ. Mixed-matrix membranes. *Angew. Chem. Int. Ed.* **2017**, *56*, 9292–9310.
24. Qiao Z, Wang Z, Zhang C, Yuan S, Zhu Y, Wang J, et al. PVAm-PIP/PS composite membrane with high performance for CO_2/N_2 separation. *AIChE J.* **2013**, *59*, 215–228.
25. James JB, Lin YS. Thermal stability of ZIF-8 membranes for gas separations. *J. Membr. Sci.* **2017**, *532*, 9–19.

26. Hu LQ, Liu JY, Zhu LX, Hou XD, Huang L, Lin HQ, et al. Highly permeable mixed matrix materials comprising ZIF-8 nanoparticles in rubbery amorphous poly(ethylene oxide) for CO_2 capture. *Separ. Purif. Technol.* **2018**, *205*, 58–65.
27. Gao YQ, Qiao ZH, Zhao S, Wang Z, Wang JX. In situ synthesis of polymer grafted ZIFs and application in mixed matrix membrane for CO_2 separation. *J. Mater. Chem. A* **2018**, *6*, 3151–3161.
28. Shen J, Liu GP, Huang K, Li QQ, Guan KC, Li YK, et al. UiO-66-polyether block amide mixed matrix membranes for CO_2 separation. *J. Membr. Sci.* **2016**, *513*, 155–165.
29. Xu R, Wang Z, Wang M, Qiao ZH, Wang JX. High nanoparticles loadings mixed matrix membranes via chemical bridging-crosslinking for CO_2 separation. *J. Membr. Sci.* **2019**, *573*, 455–464.
30. Zou C, Li Q, Hua Y, Zhou B, Duan J, Jin W. Mechanical synthesis of COF nanosheet cluster and its mixed matrix membrane for efficient CO_2 removal. ACS Appl. *Mater. Interf.* **2017**, *9*, 29093–29100.
31. Kandambeth S, Mallick A, Lukose B, Mane MV, Heine T, Banerjee R. Construction of crystalline 2D covalent organic frameworks with remarkable chemical (acid/base) stability via a combined reversible and irreversible route. *J. Am. Chem. Soc.* **2012**, *134*, 19524–19527.
32. Cheng YD, Zhai LZ, Ying YP, Wang YX, Liu GL, Dong JQ, et al. Highly efficient CO_2 capture by mixed matrix membranes containing three-dimensional covalent organic framework fillers. *J. Mater. Chem. A* **2019**, *7*, 4549–4560.
33. Fan H, Mundstock A, Feldhoff Knebel A, Gu J, Meng H, Caro J. Covalent organic framework-covalent organic framework bilayer membranes for highly selective gas separation. *J. Am. Chem. Soc.* **2018**, *140*, 10094–10098.
34. Li Y, Chung TS. Molecular-level mixed matrix membranes comprising Pebax and POSS for hydrogen purification via preferential CO_2 removal. *Int. J. Hydrogen Energy* **2010**, *35*, 10560–10568.
35. Zhao D, Ren JZ, Li H, Li X, Deng M. Gas separation properties of poly(amide-6-b-ethyleneoxide)/amino modified multi-walled carbon nanotubes mixed matrix membranes. *J. Membr. Sci.* **2014**, *467*, 41–47.
36. Cadiau A, Adil K, Bhatt PM, Belmabkhout Y, Eddaoudi M. A metal-organic framework-based splitter for separating propylene from propane. *Science* **2016**, *353*, 137–140.
37. Bhatt PM, Belmabkhout Y, Cadiau A, Adil K, Shekhah O, Eddaoudi M, et al. A fine-tuned fluorinated MOF addresses the needs for trace CO_2 removal and air capture using physisorption. *J. Am. Chem. Soc.* **2016**, *138*, 9301–9307.
38. Chen K, Xu K, Xiang L, Dong X, Han Y, Wang CQ, et al. Enhanced CO2/CH4 separation performance of mixed-matrix membranes through dispersion of sorption-selective MOF nanocrystals. *J. Membr. Sci.* **2018**, *563*, 360–370.
39. Liu GP, Cadiau A, Liu Y, Adil K, Eddaoudi M, Koros WJ, et al. Enabling Fluorinated MOF-Based Membranes for Simultaneous Removal of H_2S and CO_2 from Natural Gas. *Angew. Chem.* **2018**, *130*, 15027–15032.
40. Chen XY, Kaliaguine S. Mixed gas and pure gas transport properties of copolyimide membranes. *J. Appl. Polym. Sci.* **2013**, *128*, 380–389. doi:10.1002/app.37728.
41. Lv JY, Zhou XR, Yang JH, Wang L, Lu JM, He GH, et al. Incorporating KAUST-7 into PIM-1 towards mixed matrix membranes with long-term stable CO_2/CH_4 separation performance. *J. Membr. Sci.* **2022**, *661*, 120848.
42. Wang S, Liu Y, Huang S, Wu H, Li Y, Tian Z, et al. Pebax–PEG–MWCNT hybrid membranes with enhanced CO_2 capture properties. *J. Membr. Sci.* **2014**, *460*, 62–70.
43. Meshkat S, Kaliaguine S, Rodrigue D. Mixed matrix membranes based on amine and non-amine MIL-53(Al) in Pebax® MH-1657 for CO_2 separation. *Sep. Purif. Tech.* **2018**, *200*, 177–190.
44. Tien-Binh N, Vinh-Thang H, Chen XY, Rodrigue D, Kaliaguine S. Polymer functionalization to enhance interface quality of mixed matrix membranes for high CO_2/CH_4 gas separation. *J. Mater. Chem. A* **2015**, *3*, 15202–15213.
45. Robeson LM. The upper bound revisited. *J. Membr. Sci.* **2008**, *320*, 390–400.
46. Lin H, Van Wagner E, Freeman BD, Toy LG, Gupta RP. Plasticization-enhanced hydrogen purification using polymeric membranes. *Science* **2006**, *311*, 639–642.
47. Kanehashi S, Gu H, Shindo R, Sato S, Miyakoshi T, Nagai K. Gas Permeation and Separation Properties of Polyimide/ZSM-5 Zeolite Composite Membranes Containing Liquid Sulfolane. *J. Appl. Polym. Sci.* **2013**, *128*, 3814–3823.
48. Zhao D, Ren JZ, Li H, Hua KS, Deng MC. Poly(amide-6-b-ethylene oxide)/SAPO-34 mixed matrix membrane for CO_2 separation. *J. Energy Chem.* **2014**, *23*, 227–234.
49. Ghadimi A, Mohammadi T, Kasiri N. A novel chemical surface modification for the fabrication of PEBA/SiO_2 nanocomposite membranes to separate CO_2 from syngas and natural gas streams. *Ind. Eng. Chem. Res.* **2014**, *53*, 17476–17486.
50. Shao L, Chung TS. In situ fabrication of cross-linked PEO/silica reverse-selective membranes for hydrogen purification. *Int. J. Hydrogen Energy* **2009**, *34*, 6492–6504.
51. Chua ML, Shao L, Lowa BT, Xiao YC, Chung TS. Polyetheramine–polyhedral oligomeric silsesquioxane organic–inorganic hybrid membranes for CO_2/H_2 and CO_2/N_2 separation. *J. Membr. Sci.* **2011**, *385–386*, 40–48.
52. Jomekian A, Bazooyara B, Behbahania RM, Mohammadib T, Kargari A. Ionic liquid-modified Pebax® 1657 membrane filled by ZIF-8 particles for separation of CO_2 from CH_4, N_2 and H_2. *J. Membr. Sci.* **2017**, *524*, 652–662.
53. Abedini R, Mosayebi A, Mokhtari M. Improved CO_2 separation of azide cross-linked PMP mixed matrix membrane embedded by nano-CuBTC metal organic framework. *Process. Saf. Environ.* **2018**, *114*, 229–239.